Paper

Structure of Pores in Porous Membrane with Grafted Poly (Acrylic Acid) —Determination by Computer Simulation and Experimental Observations—

Yoshishige Okuno[1,2,*], Shaoling Zhang[3], Keiichiro Saito[3],

Hidetoshi Matsumoto[3], Mie Minagawa[3], and Akihiko Tanioka[3,*]

(Accepted 20 December 2010)

Abstract: To determine the conformation of the poly(acrylic acid) grafted on a membrane matrix, a coarse-grained particle dynamics simulation was carried out for the polymers grafted on a single cylindrical pore. It was found that the polymers grafted on the inner surface tend to occlude the pore more effectively than those grafted on the outer entrance of the pore. This suggests that the effective pore size should be controlled by the polymers grafted on the inner surface of the pore. Furthermore, the simulation showed that the grafted polymers on the inner pore surface tend to concentrate on the neighborhood of the inner pore surface, instead of spreading out towards the central axis of the pore. In the relationship between the grafted-particle density and the effective pore diameter, the calculated results are in good agreement with the experimental ones. This indicates that the membrane permeability is dependent on the effective pore size of the membrane.

Key words: Dynamics simulation; Poly (acrylic acid); Membranes; Pore materials; Coarse-grained model

1. Introduction

Synthetic membranes, which are prepared for separation tasks in the laboratory and industry, have attractive considerable attention for a long time. This is because the membranes are employed in a wide range of operations, such as microfiltration, reverse osmosis, pervaporation, gas separation, dialysis or chromatography and a lot of fields such as water purification, removal of microorganisms in dairy products, water desalination, and the dehydrogenation of natural gas, hemodialysis or the components of fuel cells. The applications depend on the type of functionality incorporated in the membrane, which can be based on the size of the pores, chemical affinity or electrostatic interactions.

The modification of the membrane matrix by grafting polymers provides an unique opportunity to modulate the interfacial properties of the membrane to improve the membrane performance

[1] AdvanceSoft Corporation, 16 th, Kowa Bldg., 1–9–20, Akasaka, Minato-ku, Tokyo 107–0052, Japan
[2] Center for Information Science, Kokushikan University, 4–28–1, Setagaya, Setagaya-ku, Tokyo 154–8515, Japan
[3] Department of Organic & Polymeric Materials, Tokyo Institute of Technology, 2–12–1–S8–27, Ookayama, Meguro-ku, Tokyo 152–8552, Japan
* Corresponding authors.
Y. Okuno; AdvanceSoft Corporation, 16 th, Kowa Bldg., 1–9–20, Akasaka, Minato-ku, Tokyo 107–0052, Japan Tel.: +81–3–5570–1682 Fax: +81–3–5570–1684
E-mail: y_okuno@advancesoft.jp
A. Tanioka; Department of Organic & Polymeric Materials, Tokyo Institute of Technology, 2–12–1–S8–27, Ookayama, Meguro-ku, Tokyo 152–8552, Japan Tel.: +81–3–5734–2426 Fax: +81–3–5734–2876
E-mail: tanioka.a.aa@m.titech.ac.jp

such as anti-fouling and environmental sensitivity[1–3]. The grafting of functional polymers on the membrane matrix offers an advantage in providing new properties to the membranes, because the variation in the polymers grafted on the membranes leads to a variety of membrane characteristics. For example, the membrane permeability is expected to be dependent on the potential of hydrogen (pH)[3–5] or temperature[6,7] of the atmosphere.

The pH-dependent membranes has attracted great interest in biology and pharmacology since its charge property and pore size can be controlled by changing pH[3]. Moreover, the transport phenomena in biophysical systems and biological applications usually include the permeation of charged molecules like amino acids and proteins, as well as ionic drugs[8–12] through membranes with pH-dependent fixed charges. As one of the pH-dependent functional monomers, the acrylic acid has been widely used in the membrane modification for the protein separation and controlled delivery systems[5,13,14]. The poly (acrylic acid)-modified membranes show a pH-sensitivity in both the membrane charge property and permeability. At a high pH, the membranes will show a negative charge due to the dissociation of the acid groups, and correspondingly pore size of the membranes is expected to decrease because of the extension of the polymer chains resulting from the electrostatic repulsion between the charged groups. In fact, the porous poly (acrylonitrile) membranes modified by grafting with poly (acrylic acid) have been prepared and characterized, and the pH-sensitivity was observed[15].

However, the structures of the grafted poly (acrylic acid) on porous poly (acrylonitrile) membranes have not been clarified in detail. Although the experimental measurements like hydraulic permeability provide some information, it still cannot determine the structures of the graft polymers in detail. Since the membrane permeability is strongly dependent on the structures of the graft polymers, the clarification of the structures of the graft polymers is important.

Therefore, in the current study, we attempted to determine the structures of the grafted polymers on porous poly (acrylonitrile) membranes by carrying out simulations. Although the pH sensitivity of the membrane is of great interest, our current attention was, as a first step of analysis, paid to the determination of the membrane structure under the neutral condition. On the basis of the simulation results, the relationship between the structure of the grafted polymer chains and the membrane permeability was discussed.

2. Method of Simulation

2.1. Coarse grained model

We used a coarse-grained model as shown in Figure 1 for the poly (acrylic acid). Each of the CH_2 and CH moieties was regarded as a single particle by introducing the united atom model. The centers of the particles were located at the carbon atoms. However, the united atom model was not applied to the carboxylic acid moiety and each atom of the acid moiety was treated as a particle. This is because the hydrogen-bonding interaction between the carboxylic acid moieties should play an important role in determining the aggregate structure of the poly (acrylic acid).

2.2. Determination of potential data

The potential-energy data for the poly (acrylic acid) were calculated using the quantum chemi-

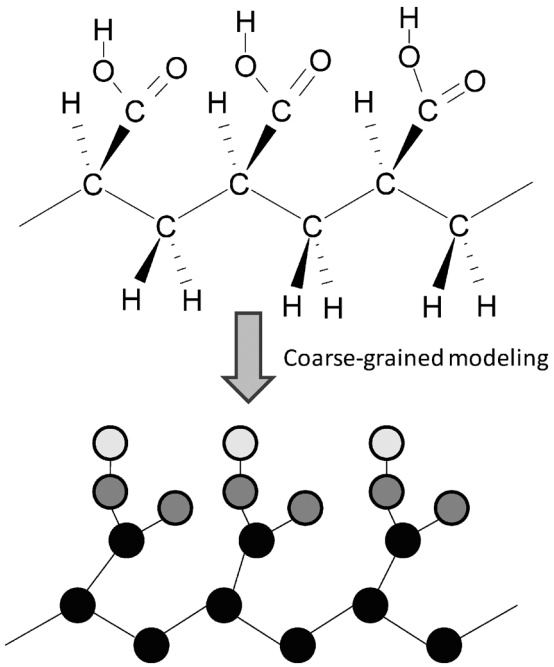

Fig. 1 The coarse-grained model for poly(acrylic acid).

cal method at the B3LYP level of theory[16] with the 6–31++G (2d, p) basis set[17], and these calculations were carried out with Gaussian03W program package[18]. This is because the potential-energy data must be predetermined to carry out the dynamics calculations following the motion of the particles on the potential-energy surface. We used the diffuse functions because the diffuse functions are very important for the estimation of the intermolecular interaction.

The total potential energy is considered to consist of the bond stretching potential, angle bending potential, torsion angle potential, nonbonding pair potential, and electrostatic potential. We introduced the following treatments to reduce the calculation cost, and we only took the angle bending potential, nonbonding pair potential, and electrostatic potential into account (shown in the following subsections).

We first introduced an approximate treatment of fixing the bond lengths during the dynamics calculation with the RATTLE method[19,20], so that the bond stretching potentials were not required here. This is accepted because the amplitude of stretching vibration is small compared with molecular dimensions.

Secondly, the torsion angle potentials were ignored here. This can be accepted because the potential-energy change accompanied by the torsion-angle change is usually very small. In fact, this ignorance has usually been applied to the coarse grained dynamics calculations.

2.2.1. Angle bending potential

The angle-bending potential-energy data were determined by the quantum chemical calculations for three small molecules that are obtained by extracting small moieties from the poly (acrylic acid) and then by capping the dangling bonds of the extracted moieties with the hydrogen atoms

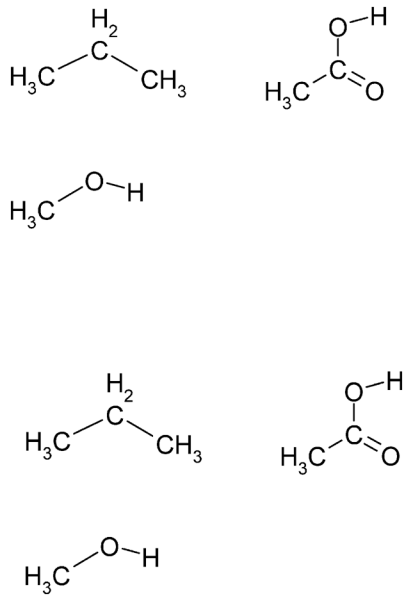

Fig. 2 The molecules that we used for determining the angle bending potentials. The propane and methanol were used for the determination of the angle bending potentials of CH_x–CH_x–CH_x and H–O–CH_x, respectively. The acetic acid was used for the determination of the angle bending potentials of CH_x–CH_x–O, CH_x–CH_x=O, and O–CH_x=O.

(Figure 2). First, stable structures were optimized for these molecules. The potential energies were then calculated for the structures with the values of cos $(\pi-\theta)=1.0, 0.9, 0.8, \ldots$, where θ is the bending angle. In these calculations, the structures were optimized except for the bending angle and the stretching bonds between the coarse-grained particles; the stretching bonds were fixed at the bond lengths of the stable structures.

The calculated results are shown in Figure 3. The angle bending potential-energy change was found to have a cosine harmonic character around the stable structure. Note that the potential energies and the corresponding force vectors at points between the discrete potential data were calculated in terms of the second-order interpolation.

2.2.2. Non-bonding pair potential

The energy data of the non-bonding pair potentials were also determined by the quantum chemical calculations for the systems consisting of two small molecules. These molecules are also regarded as the ones obtained by extracting small moieties from the poly (acrylic acid) and then by capping the dangling bonds of the extracted moieties with the hydrogen atoms (Figure 4). The total non-bonding potential was assumed to be represented by the sum of the pair interaction potentials; i.e., the H–H interaction, H–O interaction, O–O interaction, CH_x–O interaction, CH_x–H interaction, and CH_x–CH_x interaction, where CHx denotes a coarse-grained particle for every C, CH, and CH_2 moieties.

We first determined the potential-energy change accompanied by the intermolecular length change by carrying out the quantum chemical calculations. The calculations were made for each 0.01 nm increase in length of the dotted line as shown in Figure 4 from 0.1 nm to 1.0 nm, fixing the

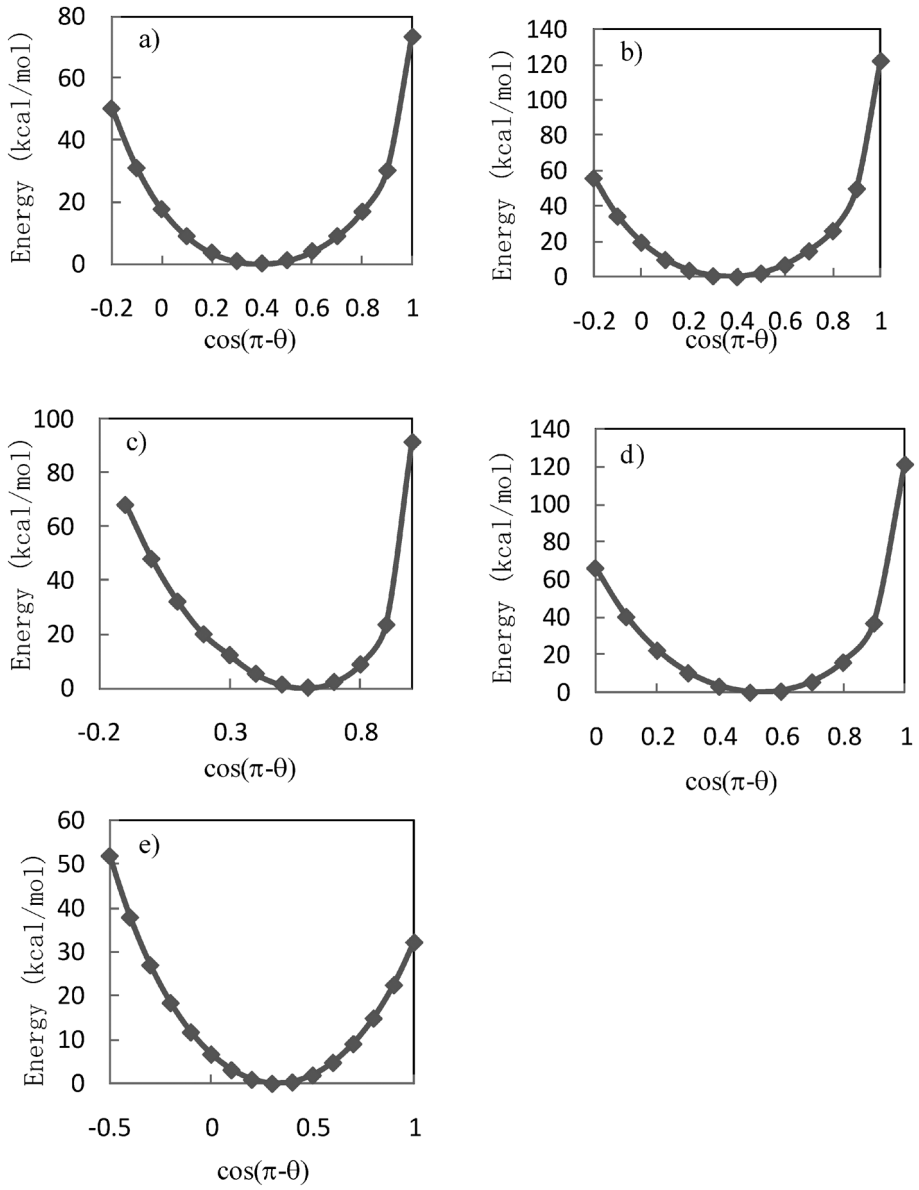

Fig. 3 a) CH_x–CH_x–CH_x angle bending potential, b) CH_x–CH_x–O angle bending potential, c) CH_x–CH_x=O angle bending potential, d) O–CH_x=O angle bending potential, and e) H–O–CH_x angle bending potential.

internal structure of each molecule and the relative orientation between the two molecules. The interaction energies were determined by subtracting the energies of the isolated molecules from the energies of the combined molecule.

We then derived the energy data of the non-bonding pair potentials between two coarse-grained particles connected by the dotted line in Figure 4 by subtracting the pair interaction energies between two coarse-grained particles that are not connected by the dotted line in Figure 4 from the interaction energies determined above. The pair interaction energies between the two coarse-

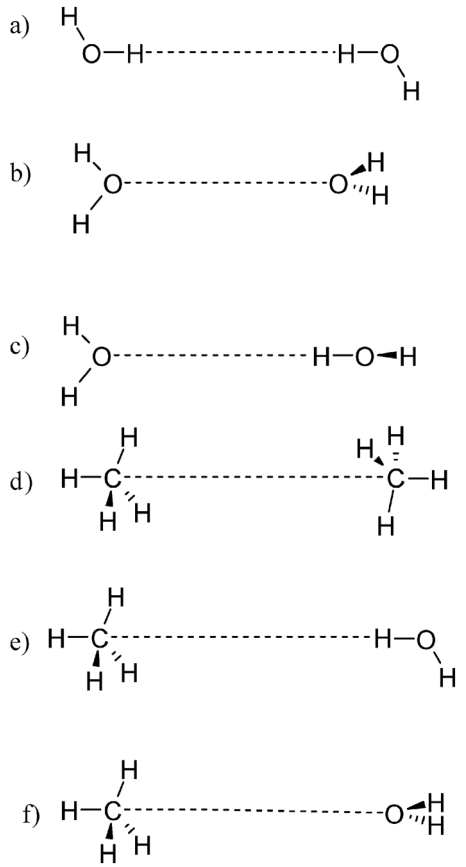

Fig. 4 The conformations we used for determining the interaction between the coarse-grained particles. The conformations a), b), c), d), e), and f) were used for the determination of the H–H, O–O, H–O, CH_x–CH_x, CH_x–H, and CH_x–O interactions, respectively.

grained particles that are not connected by the dotted line were approximated to be the Coulomb interactions between these two particles. The Coulomb interactions were determined by the interactions between the point charges of the particles. The point charges for the isolated molecules were determined by the Merz-Singh-Kollman method[21,22] in which the charges are fitted to the electrostatic potential at many points selected according to the Merz-Singh-Kollman scheme; note that this method has been used in various ways and provided satisfactory results[23]. The calculated results of the charges for CH_4, O, and H were, respectively, $0.0e$, $-0.734162e$, and $0.367081e$, where e is the elementary charge and is $1.602176487 \times 10^{-19}$ C. These results were used for the calculation of the Coulomb interaction and we finally obtained the non-bonding pair potential without the Coulomb interaction.

The calculated results are shown in Figure 5 in which potential data in the lengths between the coarse-grained-particles from 0.1 nm to 0.5 nm are depicted. The calculated potentials for the H–O, O–O, and H–H interactions were in good agreement with the potentials that were obtained for representing the water-water interaction by Kawamura[24]. Since in every case the potential energy was found to be nearly zero at 0.5 nm, the potential cut-off distance for the non-bonding pair

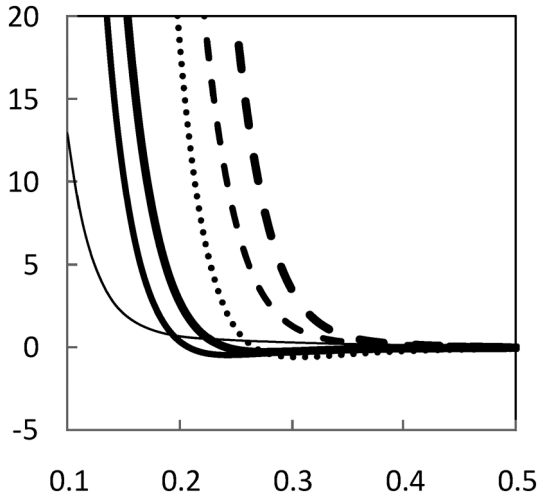

Fig. 5 Potentials of CH_x–CH_x (bold broken line), CH_x–O (broken line), O–O (dotted line), H–CH_x (bold solid line), H–O (solid line), and H–H (thin solid line).

potential was selected to be 0.5 nm.

Similar to the angle-bending potential, the second-order interpolation was used to calculate the potential energies and the corresponding force vectors at points between the discrete potential data.

2.2.3. Electrostatic interaction

For calculation of the Coulomb interaction between the grafted polymers, we first determined the charges of the poly (acrylic acid). For this, we carried out a quantum chemical calculation for the monomer unit of the poly (acrylic acid), i.e., propionic acid (CH_3CH_2COOH), and determined the charges in the coarse-grained particles, CH_3, CH_2, C, O=, O, H, where O= denotes oxygen with a double bond. The charges were determined on the basis of the Merz-Singh-Kollman method[21,22]. The determined charges were regarded as those of the corresponding polymers. The determined charges of the poly (acrylic acid) are as follows: CH_2; $-0.000729e$, CH; $0.11471e$, C; $0.574971e$, O=; $-0.532677e$, O; $-0.577577e$, H; $0.421302e$.

Using the determined charges, we can calculate the electrostatic interaction. Since the membrane is assumed to be immersed in an aqueous solution, the electrostatic interaction was calculated using the relative permittivity of water, 78.0, so that we roughly took the dielectric solvent effect into account in the simulation. This approximation was introduced to shorten the computational time, because directly treating the solvent waters results in a tremendous amount of computational time. Since the poly (acrylic acid) has a hydrophilic nature, this approximation is expected to be qualitatively acceptable. Note that the potential cut-off distance for the electrostatic interaction was selected to be 1.0 nm.

2.3. Pore model

We focused on a single pore in the membrane formed by poly (acrylonitrile) and we assumed for simplicity that the pore has a cylindrical structure. The cylindrical pore was modeled by many

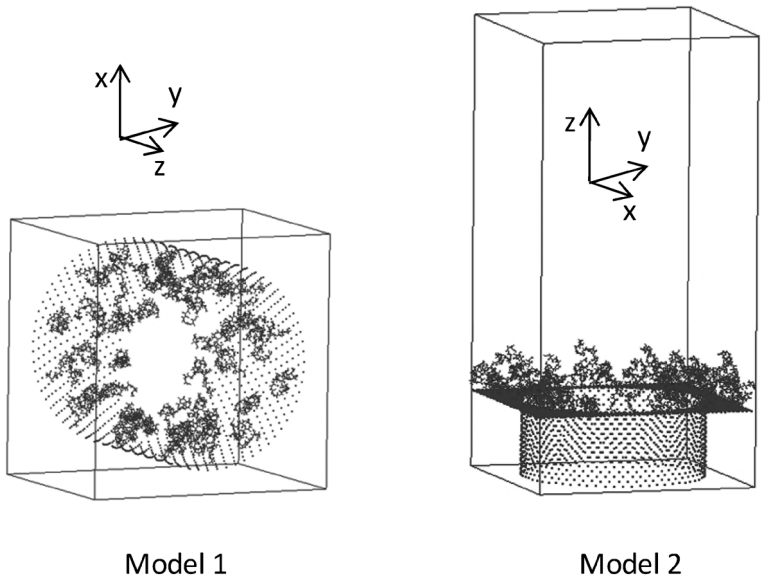

Fig. 6 Pore models. Z-axix is along the cylinder.

particles placed on the surface of the membrane. We considered two models. One is that the poly (acrylic acid) are grafted to the interior side of the cylindrical pore. The other is that the poly (acrylic acid) are grafted to the outer entrance of the pores.

In model 1 as shown in the left picture of Figure 6, the surface particles of a pore were cylindrically placed in a cell and the polymers grafted on the inner surface of the cylindrical pore. The periodic boundary condition was applied to the z axis that is along the cylinder. Sixty-four surface particles were arranged on each of the 16 lines along the circumference at equal intervals and the particles on a line along circumference and on the next line were alternated with each other in a staggered manner. The polymers were then grafted at the points arranged on each of 4 lines along the circumference at equal intervals and the grafting points on a line along the circumference and on the next line were again alternated with each other. The diameter of the cylinder was assumed to be 16.3 nm on the basis of the observed data (shown later) of the unmodified membrane. Both sides along the x-axis and y-axis of a cell are 20 nm, while the side along the z-axis was adjusted to satisfy the equal intervals of the arranged graft polymers under the periodic boundary condition.

In model 2 as shown in the right picture of Figure 6, the surface particles of a cylindrical pore were placed a way similar to model 1 except for the truncation of the cylinder, and the surface of the outer entrance of the pore was assumed to be a plane that is perpendicular to the axis along the cylindrical pore, and then the polymers graft on the outer entrance plane surface. To embody this, 64 surface particles were first arranged on each of the 16 lines (or eight lines) along the circumference at equal intervals and the particles on a line along the circumference and on the next line were alternated with each other, but the cylinder was truncated at 67.88 nm along the z-axis from the bottom of the cell. To embody the outer surface, 2045 particles are initially arranged on the 45×45 square lattice on this plane and the particles arranged on the inside of the pore were excluded from the initially arranged particles. Both sides of the x-axis and y-axis of the cell were selected to be 18.0

or 20.0 nm and a periodic boundary condition was applied to these axes, while the side of the z-axis of the cell was 40 nm and the periodic boundary condition was not imposed in this direction.

To prevent the grafted polymers from penetrating the surface, we introduced the following Lennard-Jones potential between the arranged surface particles and polymer particles;

$$U_{pore\text{-}polymer}(r_{ij}) = 4\varepsilon_{ij}\left[\left(\frac{\sigma_0}{r_{ij}}\right)^{12} - \left(\frac{\sigma_0}{r_{ij}}\right)^{6}\right] + U_{cutoff} \quad (1)$$

where, r_{ij} is the distance between the i-th surface particle and the j-th polymer particle, σ_0 is the diameter of the Lenard-Jones sphere, and ε_{ij} is the strength of the interaction. The term U_{cutoff} is chosen so that the $U_{pore\text{-}polymer}$ becomes zero at more than or equal to the cut-off distance. In the present simulation, the cut-off distance and interaction strength ε_{ij} were, respectively, selected to be 0.5 nm and 0.1 kcal/mol. The diameter of the Lenard-Jones sphere was selected to be the minimum value that makes the surface space occluded so that the polymer particles are hard to penetrate the surface. Note that this Lennard-Jones type particle wall has been used by many researchers[25,26] and has been recognized to be superior to the Lennard-Jones type flat wall used by Grest[27] in that the force along the wall surface can be taken into account.

2.4. Method of dynamics calculation

Based on the determined potential-energy data, we carried out coarse-grained particle dynamics calculations using the COGNAC engine[25] in Advance/OCTA[28,29]. To reduce the total computational cost, we divided the calculations into three steps.

We first carried out a constant temperature dynamics calculation at the high temperature of 500 K for 50 ps. This was done because the initial grafted polymer structure was arbitrarily chosen and because the calculation at high temperature should enhance slipping away from the local minimum.

Secondly, we carried out a constant temperature dynamics calculation at the room temperature of 300 K for 50 ps. This leads to the equilibrium structures at room temperature, although the viscosity effect of the medium water is not included here. We confirmed that the averaged height of the polymer particles from the inner curved surface becomes steady around 50 ps.

Finally, we carried out the Brownian dynamics calculation for 50 ps at the room temperature of 300 K where the particle motions are determined by the Langevin equation and the viscosity effect of the medium water was roughly included. To include the viscosity effect, we first determined the friction coefficient using the following equation[30]:

$$\xi = \frac{3\,\pi\eta d}{m} \quad (2)$$

where η is the viscosity, d is the diameter of the particle size, and m is the mass of the particle. We used the experimental value of the viscosity of the water, 0.00089 $kgm^{-1}\,s^{-1}$ [31]. The diameter of the particle size was selected to be the average value of the van-der-Waals diameters[32], and the mass of the particle was selected to be the averaged mass of the coarse-grained particles. As a result, the calculated frictional coefficient was determined to be $1.56 \times 10^{14}\ s^{-1}$. We also confirmed in this step that the averaged height of the polymer particles from the inner curved surface becomes steady

around 50 ps.

The other calculation conditions/technique to be common to all the jobs are as follows: the time step of the dynamics calculation is 2.5 fs, the velocity scaling method was used to make the temperature constant, the number of interval steps for the velocity scaling was selected to be 10, the RATTLE algorithm[20] was used to fix the bond lengths that are identical to the stable structure ones, and the velocity verlet algorithm was used for the time integration of the dynamics.

3. Results and discussion

3.1. Effect of the location of the grafted chains

From the calculated equilibrium structures (Figures 7 and 8) of models 1 and 2, it is found that the poly (acrylic acid) grafted on the inner curved surface narrowed the pore more effectively than that grafted on the outer plane surface around the pore entrance. This result could be easily seen by comparing M1−3 with M2−1, between which there was no significant difference in the graft particle number per surface area (Tables 1 and 2). The reason was that the grafted polymers around the pore entrance wonder about the large outer space and do not effectively contribute to the blocking of the pore.

Nielsen et al[33]. found that the hydrophilic substituent on the entrance site of the tube considerably enhanced the water transport, and they suggested that the main factor, which governed the transport property, was the nature of the substance around the entrance. In their case, the diameter of the tube was as small as ca. 1.3 nm, so that the interaction between the transmitting water and the entrance substance is quite important. However, in our case the cylindrical pore has much larger diameter of 16.3 nm, so the effect found by Nielsen et al. can be neglected in the present cases. But, note that the present results just show that the polymers grafted on the inner curved surface narrowed the pore more effectively than those grafted on the outer plane surface around the pore entrance and do not necessarily show that the grafted polymers around the pore entrance have no effect on the transport property.

The result mentioned above indicates that the determining factor in the membrane permeability should be the polymers grafted on the inner curved surface of the pore rather than those grafted on the outer surface around the pore entrance. Therefore, from here on, more attention will be paid to model 1, i.e., the polymers grafted on the inner curved surface of the cylindrical pore.

3.2. Effect of number of the grafted polymers

From the calculations for the model 1 (Figure 7), it is also found that the polymers grafted on the inner pore surface tend not to spread out toward the center of the pores, but to concentrate in the neighborhood of the circumferential surface of the cylindrical pores. This phenomenon can be explained as follows.

On one hand, each polymer tends to wonder just around the grafting point unless the distance between the neighboring grafting points is smaller than the gyration diameter of the polymers. The gyration radius R_G is a parameter showing the spatial extension of a polymer chain, and is defined as the root mean square of the distance between each atom and the center of mass of the polymer chain. The gyration radius is given by the following equation[34]:

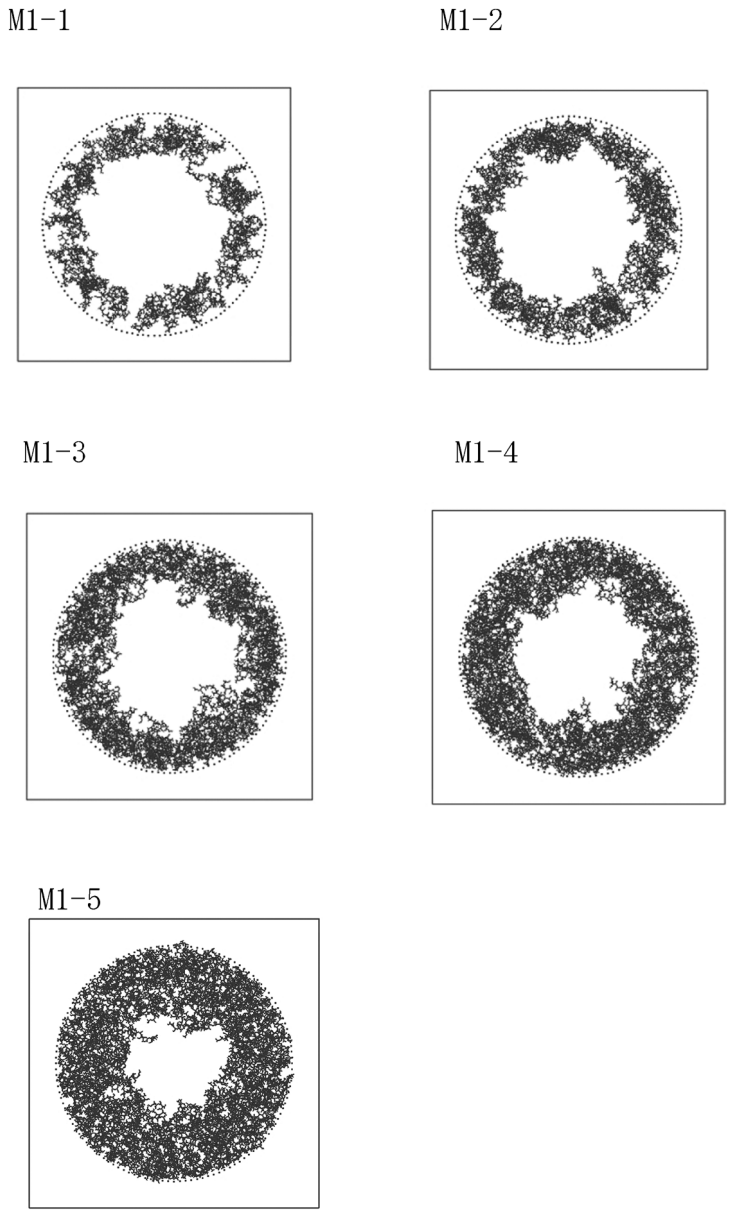

Fig. 7 Equilibrium structures for model 1. The job labels correspond to those denoted in Table 1.

$$\langle R_G^2 \rangle = \frac{1}{N} \int \sum_{i=1}^{N} (\mathbf{r}_i - \mathbf{r}_G)^2 \text{'} \qquad (3)$$

where $\mathbf{r}_i$ and $\mathbf{r}_G$ are the i-th particle position vector and the position vector of the center of mass of the polymer, respectively. Using Equation (3), the average diameter $2\langle R_G^2 \rangle^{1/2}$ were estimated from the simulations to be 2.09–2.86 nm (Table 1). The average distances between the neighboring grafting points for M1–1, M1–2. M1–3, M1–4, and M1–5, which are inversely proportional to the

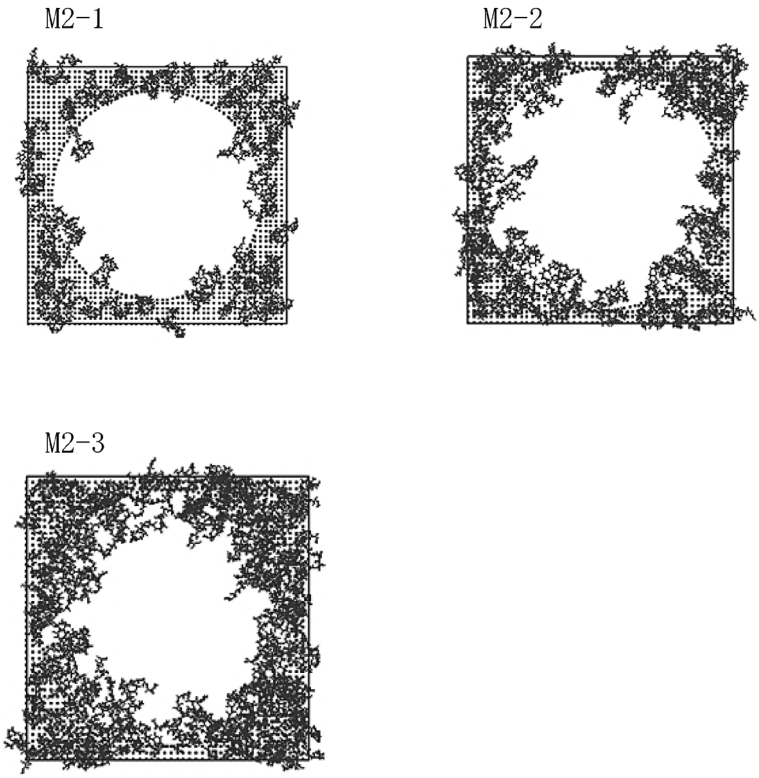

Fig. 8 Equilibrium structures for model 2. The job labels correspond to those denoted in Table 2.

Table 1 Calculation conditions and results for model 1.

Model	Number of graft polymers	Degree of polymerization	Cell size along cylinder (nm)	Particle number per surface area (particle/nm^2)	σ_0 (nm)	Effective pore diameter (nm)	$2\langle R_G^2\rangle^{1/2}$ (nm)
M1-1	44 (4×11) [a]	40	16.13	12.78	6.72	16.3	2.09
M1-2	64 (4×16) [a]	40	11.09	27.06	4.62	16.3	2.26
M1-3	92 (4×23) [a]	40	7.71	55.92	3.21	12.3	2.37
M1-4	108 (4×27) [a]	40	6.57	77.04	2.74	10.3	2.45
M1-5	128 (4×32) [a]	40	5.54	108.29	2.31	8.0	2.85

[a] First number in parenthesis denotes the number of lines of graft points along the circumference and the second number denotes the number of graft polymers on each line.

Table 2 Calculation conditions and results for model 2.

Model	Number of graft polymers	Degree of polymerization	Cell size (nm)	Particle number per surface area (particle/nm^2)	Particle numbers on surface	σ_0 (nm)
M2-1	48	40	20×20×40	60.24	2219	2.83
M2-2	60	40	18×18×40	124.86	1753	2.83
M2-3	92	40	18×18×40	191.46	1753	2.83

square root of the grafting density, are 4.33, 2.98, 2.07, 1.77, 1.49 nm, respectively[35]. Since the average distances for M1–1 and M1–2 are actually greater than the gyration diameters, the polymer chains hardly overlap each other. Under such circumstance, the repulsive excluded-volume interaction does not occur between the polymers, so they wonder just around the grafting points. Since the average distances for M1–3, M1–4 and M1–5 are less than the gyration diameters, the polymer chains overlap each other. Under such circumstance, the repulsive excluded-volume interaction occurs between the polymers, so they somewhat stretch in the direction perpendicular to the circumferential surface, but this stretch should occur after filling the neighborhood of the circumferential surface with the particles.

On the other hand, the electrostatic interaction between the grafted polymers is also expected to contribute to the concentration of the polymers. However, this contribution is limited. This is because the poly (acrylic acid) are immersed in the waters with a high dielectric constant. Although the carboxyl groups have a strong attractive electrostatic force, this interaction should be effectively weakened due to the waters existing between the polymers.

As a result, the pore remains with a clear circular form, when the number of the graft polymers is moderate. The diameter of the remaining hole can be regarded as the effective pore diameter. The membrane permeability is therefore expected to be dependent on this diameter.

3.3. Effect of degree of polymerization

To examine the relationship between the degree of polymerization and the effective pore size, the structures for the models in case of lower degree of polymerization were calculated. the calculated structures are shown in Figure 9. It was found that the remaining hole of M1–4′ (Figure 9) is larger than that of M1–5 (Figure 7), which has similar particle number per surface area but higher polymerization degree. This finding indicates that the effective pore diameter is dependent on not only the particle number per surface area but also on the degree of polymerization.

Using Equation (3), the average gyration diameters $2\langle R_G^2\rangle^{1/2}$ were estimated from the simulations to be 1.63–2.20 nm (Table 3). The average distances between the neighboring grafting points for M1–1′, M1–2′. M1–3′, M1–4′, and M1–5′ are 1.99, 1.49, 1.25, 1.08, 0.95 nm, respectively. Since the average distances for M1–2′, M1–3′, M1–4′, and M1–5′ are actually less than the gyration diameters, the polymer chains overlap each other. Under such circumstance, the repulsive excluded-volume interaction occurs between the polymers, so that they can stretch in the direction perpendicular to the circumferential surface.

The calculated particle densities as a function of the distance from the central axis of the pore are shown in Figure 10. The examination of the particle densities as a function of the distance from the central axis of the pore shows that the region in the neighborhood of the circumference surface seems to be nearly saturated with the polymer particles for M1–5′, because there is a plateu in Figure 10b from 9 nm to 16 nm. The saturated particle density is about 50.0 particle/nm^3 that corresponds to ca 1.0 g/cm^3. Thus, we defined the effective diameter of the hole, which remained unoccupied with polymers, as twice the distance between the central axis of the cylindrical pore and the circularly sliced region where the particle density is greater than 25.0 particle/nm^3, half of the saturated particle density.

The calculated results (Table 3) in lower polymerization degrees are consistent with the ex-

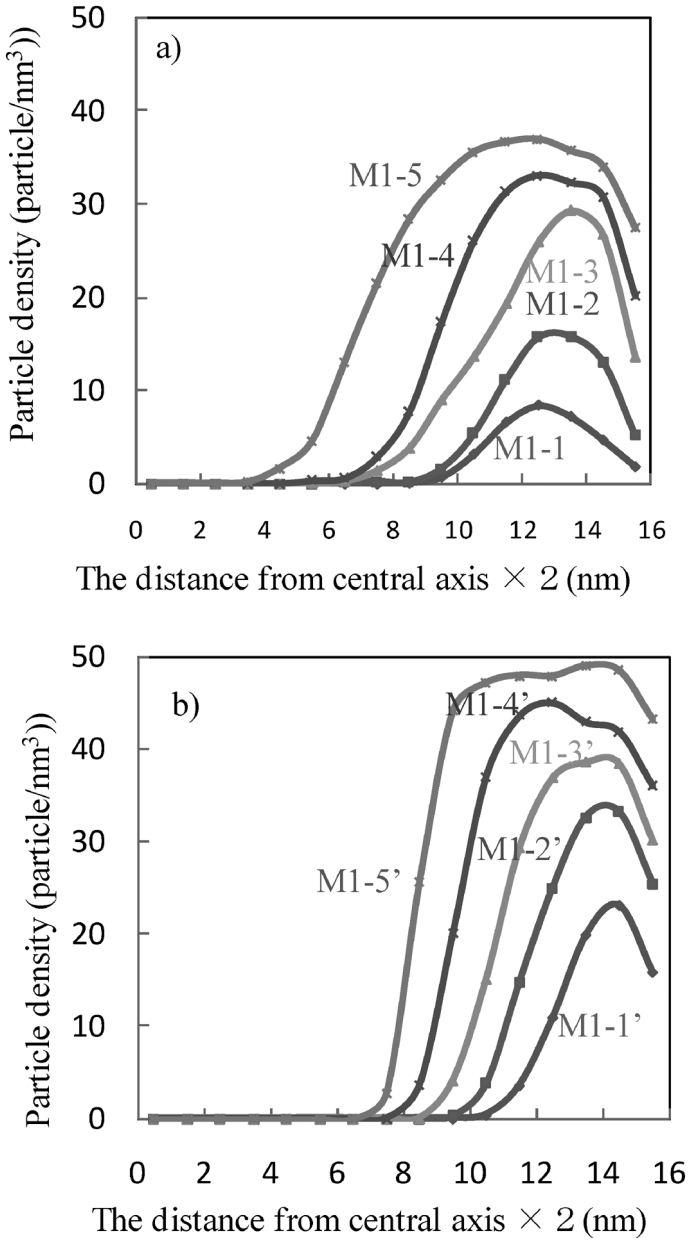

Fig. 9 Equilibrium structures for model 1 with small degree of polymerization. The job labels correspond to those denoted in Table 3.

perimental results of the hydraulic permeability of the poly (acrylic acid) grafted on membranes (Table 4); here the detail of the experiment is shown in Ref. 17 and summarized in Appendix. First, the pore diameter estimated from the calculation for the M1−2′, 12.5 nm, is 2.7 nm larger than that for the M1−4′, 9.8 nm; the particle number per surface area ratio of M1−2′ to M1−4′ is 0.53. Second, the pore diameter of AAc−1, 12.7 nm, estimated from the hydraulic permeability (as shown

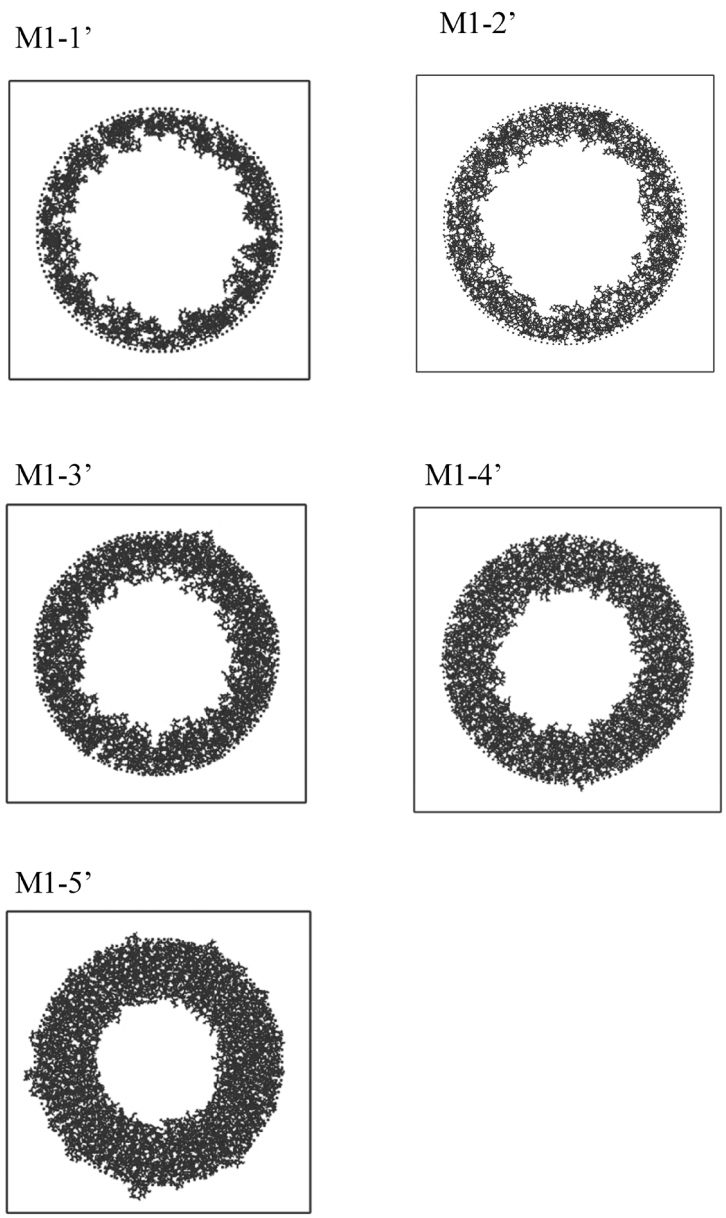

Fig. 10 The particle density versus the distance from the central axis of the cylindrical pore.

in Table 4, together with the physicochemical properties of the modified membranes) is greater by 3.0 nm than that of AAc–2, 9.7 nm; the net charge density ratio of AAc–1 to AAc–2, which are expected to be proportional to the particle number per surface area, was 0.49. The observed dependence of the effective pore diameter on the particle number per surface area is in good agreement with the calculated one. This agreement validates the structures of the graft polymers on the membrane matrix are the ones shown in Figure 9 and that the transport properties are dependent on the effective pore size of the membrane.

Table 3 Calculation conditions and results for model 1 with small degree of polymerization.

Model	Number of graft polymers	Degree of polymerization	Cell size along cylinder (nm)	Particle number per surface area (particle/nm^2)	σ_0 (nm)	Effective pore diameter (nm)	$2\langle R_G^2\rangle^{1/2}$ (nm)
M1–1′	96 (4×24) [a]	21	7.39	31.96	3.08	16.3	1.63
M1–2′	128 (4×32) [a]	21	5.54	56.82	2.31	12.5	1.75
M1–3′	152 (4×38) [a]	21	4.67	80.09	1.95	11.2	1.85
M1–4′	176 (4×44) [a]	21	4.03	107.46	1.68	9.8	2.02
M1–5′	200 (4×50) [a]	21	3.55	138.62	1.48	8.5	2.20

[a] First number in the parenthesis denotes the number of lines of graft points along the circumference and the second number denotes the number of graft polymers on each line.

Table 4 Physicochemical properties of the poly(acrylic acid) modified membranes[17] (See Appendix).

	DG[a] (w/w%)	Net charge density[b] (*10^{-5} mol/g)	Contact angle[c] (°)	Hydraulic permeability (ml*m^{-2}*h^{-1}*cm^{-1} H_2O)	Estimated pore size[d] (nm)
AAc–1	0.53	6.87	52	695	12.7
AAc–2	1.38	13.9	53	237	9.7
AAc–3	4.86	24.8	52	79	7.4
Unmodified PAN	—	—	56	1895	16.3[e]

[a] Degree of graft polymerization, which is defined in Equation (A–1).
[b] Measured by the potentiomeric titration method.
[c] Dynamic sessile drop method measured with deionized water at pH 5.6.
[d] Pore size of the membranes was calculated from the hydraulic permeability by the Hagen-Poiseuille equation at pH 7.4.
[e] Measured by capillary condensation method.

4. Conclusion

By carrying out the coarse-grained dynamics simulations for the poly (acrylic acid) grafted on a pore surface, it was found that the polymers grafted on the inner wall occlude the pore more effectively than those grafted on the outer entrance wall, and that the polymers grafted on the inner pore surface not to spread out toward the center of the pore, but to concentrate in the neighborhood of the inner wall. These findings lead to the conclusion that the membrane permeability is dependent on the effective size of the pore that remains unoccupied by the grafted polymers, which is more affected by the polymers grafted on the inner wall of the pores.

Note that although several assumptions were made in the calculation, such as the chosen degree of polymerization, the calculation gave an insight into the relationship between the grafted polymer chains and the pore structure, and their effects on the membrane permeability.

Acknowledgements

YO thanks Dr. K. Matsubara for his encouragement.

Appendix: Experimental Part

A.1. Preparation of poly (acrylonitrile) membrane

Poly (acrylonitrile) (PAN) membrane were prepared by the phase inversion method. A mixed solution of 8.0 wt.–% PAN (M_w 410,000) powder and 2.0 wt.–% poly (vinylpyrrolidone) (PVP, M_w 40,000) in N,N–dimethyleformamide (DMF) was stirred at 343 K for 5 h and then subsequently cooled to 298 K. The polymer solution was cast onto a glass plate guided by a 200–μm thick spacer. After evaporating the solvent for 30 s at 298 ± 1 K, the plate was immersed in a coagulation medium (40 vol% glycerol and water mixture) for 20 min at 293 K. The membrane was removed from the plate and washed with abundant deionized water for 3 days to remove the PVP before the following experiments. The obtained PAN membrane had a thickness of about100 μm, average pore size of 16.3 nm (measured by capillary condensation method), and a hydraulic permeability of 1895 $ml \cdot m^{-2} \cdot h^{-1} \cdot cm^{-1}$ H_2O.

A.2. Graft polymerization

Graft polymerization onto the PAN membrane pore surfaces was performed by initiation of a redox system[36] and the procedure is as follows: the membranes were immersed in the acrylic-acid monomer solution and the dissolved oxygen was removed by flowing nitrogen gas; the solution was kept in a reciprocating shaker for 1 h at 298 K after the addition of the $FeSO_4$ reduction reagent; the graft polymerization was then initiated by the addition of hydrogen peroxide as the oxidation reagent. After the graft polymerization, membranes were washed with abundant deionized water for 24 h at 298 K and subsequently with 1 mN HCl and 0.1 mN NaOH to remove the homopolymer produced simultaneously in the graft polymerization.

The degree of graft polymerization (DG) was calculated using the following equation:

$$DG = \frac{W_2 - W_1}{W_1} \qquad (A\text{–}1)$$

where W_1 is the weight of the dried membrane before graft polymerization and W_2 is that of the dried membrane after graft polymerization.

A.3. Hydraulic permeability measurements

The hydraulic permeability of the membranes was calculated from the flow rate of the deionized water after elution for 20 min at 298 K with a constant hydrostatic pressure difference of 100 kPa across the membrane. The membrane area exposed to the flow was 3.8 cm^2.

A.4. Estimation of pore size of the membranes

The Hagen-Poiseuille equation[37,38] was usually used to calculate the pore size of the membranes as follows:

$$J = \frac{\varepsilon r^2}{8\,\eta\tau}\frac{\Delta P}{\Delta x} \qquad (A\text{–}2)$$

where J is the flux of water, η is the viscosity of water, ΔP, and Δx are the pressure difference and membrane thickness, respectively, r and τ are the pore size and the tortuosity factor of the mem-

brane, respectively, ε is the surface porosity, which is the fractional pore area (ε is equal to the ratio of the pore area to membrane area A_m multiplied by the number of pores n_p, $\varepsilon = n_p \pi r^2 / A_m$).

In our case, the pore size of the modified membranes was estimated from that of the unmodified membrane by assuming that the pore number and thickness of the membrane did not change after grafting, shown as

$$\frac{J}{J_0} = \left(\frac{r}{r_0}\right)^4 \qquad (A\text{-}3)$$

where J_0 and r_0 are the hydraulic permeability and pore size of the unmodified membrane, respectively.

References

1 A. Bhattacharya and B. N. Misra, Prog. Polym. Sci., 29 (2004) 767.
2 Y. Ito, Y. Ochiai, Y. Park, and Y. Imanishi, J. Am. Chem. Soc., 119 (1997) 1619.
3 J. Hautojärvi, K. Kontturi, J. Näsman, B. Svarfvar, P. Viinikka, and M. Vuoristo, Ind. Eng. Chem. Res., 35 (1996) 450.
4 Y. S. Park, Y. Ito, and Y. Imanishi, Chem. Mater., 9 (1997) 2755.
5 H. Zhang, and Y. Ito, Langmuir, 17 (2001) 8336.
6 L. Ying, E. T. Kang, K. G. Neoh, Langmuir, 18 (2002) 6416.
7 L. Ying, E. T. Kang, K. G. Neoh, K. Kato, H. Iwata, Macromol. Mater. Eng., 288 (2003) 11.
8 T. Jimbo, P. Ramírez, A. Tanioka, S. Mafé, and N. Minoura, Journal of Colloid and Interface Sci., 225 (2000) 447.
9 J. Ku, S. Lai, N. Heri, P. Ramírez, S. Mafé, and P. Stroeve, J. Phys. Chem. C, 111 (2007) 2965.
10 J. Ku, and P. Stroeve, Langmuir, 20 (2004) 2030.
11 K. Chun, and P. Stroeve, Langmuir, 18 (2002) 4653.
12 P. Ramírez, A. Alcaraz, S. Mafé, and J. Pellicer, J. Colloid and Interface Sci., 253 (2002) 171.
13 L. Chu, Y. Li, J. Zhu, H. Wang, and Y. Liang, J. Control. Release, 97 (2004) 43.
14 J. Shim, Y. B. Lee, Y. M. Lee, J. App. Poly. Sci., 74 (1999) 75.
15 S. Zhang, Study on Insulin Transport across Porous Charged Membranes, Thesis in Tokyo Institute of Technology, 2008.
16 A. D. Becke, J. Chem. Phys., 98 (1993) 5648.
17 J. S. Binkley, J. A. Pople, and W. J. Hehre, J. Am. Chem. Soc., 102 (1980) 939.
18 M. J. Frisch, G. W. Trucks, H. B. Schlegel, G. E. Scuseria, M. A. Robb, J. R. Cheeseman, J. A. Montgomery, Jr., T. Vreven, K. N. Kudin, J. C. Burant, J. M. Millam, S. S. Iyengar, J. Tomasi, V. Barone, B. Mennucci, M. Cossi, G. Scalmani, N. Rega, G. A. Petersson, H. Nakatsuji, M. Hada, M. Ehara, K. Toyota, R. Fukuda, J. Hasegawa, M. Ishida, T. Nakajima, Y. Honda, O. Kitao, H. Nakai, M. Klene, X. Li, J. E. Knox, H. P. Hratchian, J. B. Cross, V. Bakken, C. Adamo, J. Jaramillo, R. Gomperts, R. E. Stratmann, O. Yazyev, A. J. Austin, R. Cammi, C. Pomelli, J. W. Ochterski, P. Y. Ayala, K. Morokuma, G. A. Voth, P. Salvador, J. J. Dannenberg, V. G. Zakrzewski, S. Dapprich, A. D. Daniels, M. C. Strain, O. Farkas, D. K. Malick, A. D. Rabuck, K. Raghavachari, J. B. Foresman, J. V. Ortiz, Q. Cui, A. G. Baboul, S. Clifford, J. Cioslowski, B. B. Stefanov, G. Liu, A. Liashenko, P. Piskorz, I. Komaromi, R. L. Martin, D. J. Fox, T. Keith, M. A. Al-Laham, C. Y. Peng, A. Nanayakkara, M. Challacombe, P. M. W. Gill, B. Johnson, W. Chen, M. W. Wong, C. Gonzalez, and J. A. Pople, Gaussian 03, Revision E.01, Gaussian, Inc., Wallingford CT, 2004.
19 H. C. Anderson, J. Comput. Phys., 52 (1983) 24.
20 M. P. Allen and D. J. Tildesley, Computer Simulation of Liquids, Oxford Scientific Publications, Oxford, 1989.
21 B. H. Besler, K. M. Merz Jr., and P. A. Kollman, J. Comp. Chem., 1 (1990) 431.
22 U. C. Sigh and P. A. Kollman, J. Comp. Chem., 5 (1984) 129.
23 Y. Okuno, T. Yokoyama, S. Yokoyama, T. Kamikado, and S. Mashiko, J. Am. Chem. Soc., 124 (2002) 7218.
24 Y. Kawamura, Teion Kagaku (in Japanese), 164 (2005) 3.
25 T. Aoyagai, F. Sawa, T. Shoji, H. Fukunaga, J. Takimoto, and M. Doi, Comput. Phys. Comm. 145 (2002) 267.
26 S. Maruyama and T. Kimura, Proceedings of the 5th ASME/JSME Thermal Engineering Joint Conf., p. 1 and the references therein.
27 G. S. Grest, J. Chem. Phys. 105 (1996) 5532.
28 see the Adavance/OCTA web site http://www.advancesoft.jp/product/advance_octa/(in Japanese). The Advance/

OCTA is a commercial version of OCTA that was functionally extended by the AdvanceSoft Corporation.
29 see the OCTA web site http://octa.jp/
30 J. -P. Hansen and I. R. McDonald, Theory of Simple Liquid, 2nd Ed., Academic Press, London, 1986.
31 David R. Lide, ed., ''CRC Handbook of Chemistry and Physics'', 73rd Edition, CRC Press/Taylor and Francis, Boca Raton, FL, 1992.
32 see the web site of http://www.chem.nara-wu.ac.jp/~tanase/echem/PeriodicTable/Element1/
33 S. O. Nielsen, C. F. Lopez, G. Srinivas, and M. L. Klein, J. Phys.: Condens. Matter, R481 (2004) 16.
34 T. Kawakatsu, Statistical Physics of Polymers, Springer, Berlin, 2001.
35 Here we neglected the effect of the curvature for the simplicity of the discussion. In the discussion of the overlap of the R_G, the curvature of the grafting cylinder may be also important. Considering the average gyration diameter $2\langle R_G^2\rangle^{1/2}$ of 2.09–2.86 nm, the center of the mass of the polymer is 1.045–1.43 nm from the curved surface. Then the average distances between the neighboring- polymer centers for M1–1′, M1–2′. M1–3′, M1–4′, and M1–5′ become 4.07, 2.76, 1.88, 1.63, 1.35 nm, which are somewhat smaller than the averaged distances between the neighboring grafting points , 4.33, 2.98, 2.07, 1.77, 1.49 nm. This shows that the curvature increases the overlapping of the R_G, but its effect is limited in the present cases.
36 T. Jimbo, M. Higa, N. Minoura, and A. Tanioka, Macromolecules, 31 (1998) 1277.
37 M. Mulder, Basic principles of membrane technology, 2nd edition, Kluwer academic publishers, Dordrecht, Boston, London, Chapter IV, p170
38 H. Matsumoto, Y. Koyama, and A. Tanioka, Colloid and Surfaces A: Physicochem. Eng. Aspects, 222 (2003) 165.